Preclinical Development of ADCT-601, a Novel Pyrrolobenzodiazepine Dimer-based Antibody–drug Conjugate Targeting AXL-expressing Cancers

Francesca Zammarchi[1], Karin EG. Havenith[1], Simon Chivers[1], Paul Hogg[1], Francois Bertelli[2], Peter Tyrer[2], Narinder Janghra[3], Halla W. Reinert[3], John A. Hartley[3], and Patrick H. van Berkel[1]

ABSTRACT

AXL, a tyrosine kinase receptor that is overexpressed in many solid and hematologic malignancies, facilitates cancer progression and is associated with poor clinical outcomes. Importantly, drug-induced expression of AXL results in resistance to conventional chemotherapy and targeted therapies. Together with its presence on multiple cell types in the tumor immune microenvironment, these features make it an attractive therapeutic target for AXL-expressing malignancies.

ADCT-601 (mipasetamab uzoptirine) is an AXL-targeted antibody–drug conjugate (ADC) comprising a humanized anti-AXL antibody site specifically conjugated using GlycoConnect technology to PL1601, which contains HydraSpace, a Val-Ala cleavable linker and the potent pyrrolobenzodiazepine (PBD) dimer cytotoxin SG3199. This study aimed to validate the ADCT-601 mode of action and evaluate its efficacy *in vitro* and *in vivo*, as well as its tolerability and pharmacokinetics.

ADCT-601 bound to both soluble and membranous AXL, and was rapidly internalized by AXL-expressing tumor cells, allowing release of PBD dimer, DNA interstrand cross-linking, and subsequent cell killing. *In vivo*, ADCT-601 had potent and durable antitumor activity in a wide variety of human cancer xenograft mouse models, including patient-derived xenograft models with heterogeneous AXL expression where ADCT-601 antitumor activity was markedly superior to an auristatin-based comparator ADC. Notably, ADCT-601 had antitumor activity in a monomethyl auristatin E–resistant lung-cancer model and synergized with the PARP inhibitor olaparib in a BRCA1-mutated ovarian cancer model. ADCT-601 was well tolerated at doses of up to 6 mg/kg and showed excellent stability *in vivo*.

These preclinical results warrant further evaluation of ADCT-601 in the clinic.

Introduction

AXL is a transmembrane receptor that is part of the TAM (TYRO3, AXL, and MER) family of tyrosine kinase receptors. The AXL protein comprises an extracellular domain with two immunoglobulin (Ig)-like motifs, two fibronectin type III motifs, and an intracellular tyrosine kinase domain (1, 2). AXL activation is mediated partly through interaction with the growth arrest specific 6 (GAS6) ligand. AXL activation triggers a series of signal transduction and biological effects including immune suppression, cell survival, proliferation, migration, and adhesion (2, 3).

AXL has numerous roles in the development and progression of cancer. It is overexpressed in many solid tumors (4, 5) and hematologic malignancies (6), with overexpression of AXL maintained in both primary tumors and metastases (3). AXL expression in normal tissue is reported to be significantly lower than in tumor tissue (7, 8).

As a downstream effector of epithelial-to-mesenchymal transition, AXL enhances the invasive mobility of cancer cells; hence AXL expression is associated with increased metastasis and poor prognosis (9–11). Several lines of evidence support a role for AXL in promoting angiogenesis and enabling tumor growth (3, 7). AXL overexpression on multiple cell types in the tumor immune microenvironment, including M2 macrophages, supports tumor immune escape as AXL signaling stimulates an immunosuppressive chemokine profile and promotes a suppressive myeloid microenvironment (12, 13).

Importantly, drug-induced expression of AXL results in resistance to conventional chemotherapy and targeted therapies (14). Increased expression and activation of AXL was observed in EGFR-mutated lung cancer cells with acquired erlotinib resistance (15, 16). Prolonged treatment of renal cell carcinoma cell lines with sunitinib increased activation of AXL, and inhibition of AXL overcame acquired resistance to sunitinib (17). Similarly, increased AXL levels and activation have been observed in imatinib-resistant chronic myeloid leukemia cells, lapatinib-resistant HER2-positive breast tumor cells, and cisplatin-resistant ovarian cancer cells (18–20).

The diverse role of AXL in facilitating cancer progression, and its presence on immunosuppressive cell types in the tumor immune microenvironment, make it an attractive therapeutic target (2, 21). For example, the AXL-specific inhibitor bemcentinib (BGB324) is in clinical development for the treatment of non–small cell lung cancer (NSCLC), acute myeloid leukemia, and metastatic melanoma (21–23).

Antibody–drug conjugates (ADCs) are of increasing importance as a new class of antitumor therapeutics delivering highly potent cytotoxic agents via monoclonal antibodies (mAbs) that target tumor-associated antigens (24). Two AXL-specific ADCs that have been in early clinical development for the treatment of various solid tumors are enapotamab vedotin [HuMax-AXL-ADC/AXL-107- monomethyl

[1]ADC Therapeutics (UK) Limited, London, United Kingdom. [2]AstraZeneca (MedImmune/Spirogen), Cambridge, United Kingdom. [3]UCL Cancer Institute, London, United Kingdom.

Note: Supplementary data for this article are available at Molecular Cancer Therapeutics Online (http://mct.aacrjournals.org/).

Corresponding Author: Francesca Zammarchi, Imperial College White City Campus, ADC Therapeutics (UK) Limited, London W12 0BZ, United Kingdom. E-mail: francesca.zammarchi@adctherapeutics.com

Mol Cancer Ther 2022;21:582–93

doi: 10.1158/1535-7163.MCT-21-0715

auristatin E (MMAE); NCT02988817; since terminated] (24, 25), and CAB-AXL-ADC (BioAtla, LLC; NCT03425279), which is based on conditionally active binding (CAB) technology (26).

ADCT-601 (mipasetamab uzoptirine) is an ADC comprising a humanized IgG1 antibody against human AXL site-specifically conjugated using GlycoConnect™ technology to PL1601, which contains HydraSpace™, a Val-Ala cleavable linker and the pyrrolobenzodiazepine (PBD) dimer cytotoxin SG3199 (27–29). PBD dimers represent a potent new class of toxins that bind in the minor DNA groove and form potent, sequence-selective, cytotoxic DNA interstrand crosslinks (ICLs), which result in a stalled DNA replication fork, blocking cell division and causing cell death (30). GlycoConnect™ is a promising next-generation ADC conjugation technology that delivers site-specific, stable, and highly efficacious ADCs (28), particularly in combination with HydraSpace™ spacer technology (27).

This study characterized the mode of action of ADCT-601 when used as monotherapy, both *in vitro* and *in vivo*, in tumor models of different origins, and in combination with olaparib in a BRCA1-mutated ovarian cancer model; the safety and tolerability of ADCT-601 in rats were also evaluated.

Materials and Methods

Synthesis of ADC

Anti-human AXL murine IgG2b mAb (1H12; in-licensed from BerGenBio ASA) was generated by the procedure described previously (31). Humanization of 1H12 was performed by grafting the complementarity-determining region of the murine 1H12 antibody into human IgG1 frameworks to generate 1H12-HAKB.

1H12-HAKB was prepared for site-specific conjugation using GlycoConnect™ technology (Synaffix). After enzymatic trimming of the N-linked glycans in the Fc pocket of antibody, the terminal GlcNAc was extended with 6-N_3-GalNAc using GalNAc-transferase, allowing metal-free click conjugation of the payload PL1601 (28). The PL1601 payload is a bicyclo(6.1.0)non-4-yne (BCN)-HydraSpace™ linker analog of SG3249 (32), comprising HydraSpace™ (27), a protease Val-Ala cleavable linker and the PBD dimer cytotoxin SG3199, as shown in **Fig. 1A**. The resulting ADC was designated as ADCT-601 (**Fig. 1A**).

B12-PL1601 was generated by conjugating a nonbinding isotype-control antibody, B12 (anti-HIV gp120), to the PL1601 payload following the same procedure described for 1H12-HAKB.

ADC AXL-107-MMAE was generated by Sterling Pharma Solutions, as described previously (25).

Characterization of ADCT-601

Characterization of ADCT-601 was performed by size exclusion chromatography and reduced reverse-phase liquid chromatography, using standard techniques as described previously (33, 34).

Human cell lines

The cell lines used in this study were purchased commercially (ATCC and DMSZ), except for SN12C which was obtained from the NCI (Supplementary Table S1). Each cell line used in *in vitro* experiments was between passage number 5 and 25. No additional *Mycoplasma* or authentication tests were performed in addition to what done by the supplier.

AXL cell surface density

Cell surface AXL density was determined using Quantum Simply Cellular Kit (Bangs Laboratories) per manufacturer's instructions. Specific antibody binding density was calculated from the antibody-binding capacity (ABC) of cells stained with 1H12-HAKB minus the ABC of cells stained with the nonbinding isotype control antibody B12.

In vitro binding

Surface plasma resonance

Surface plasma resonance was used to measure the binding affinity and kinetics of 1H12-HAKB to the human TAM receptors AXL, MER, and TYRO3, the binding affinity of 1H12-HAKB and ADCT-601 to the soluble recombinant extracellular domain of human AXL (sAXL), and the equilibrium binding constant (K_D) from steady-state measurements for the interaction of all human Fc-gamma receptors (FcγRs-I, -IIA, -IIB, -IIIA-158V, and -IIIA-158F) and human neonatal Fc receptor (FcRn) with 1H12-HAKB and ADCT-601. The binding of each of the FcγR concentration series and FcRn were measured against immobilized 1H12-HAKB or ADCT-601. K_D values were obtained from at least three independent kinetic runs per test item and calculated with BIA evaluation software (GE Healthcare). Instrumentation settings are provided in Supplementary Materials and Methods.

Flow cytometry

The binding of 1H12-HAKB for membranous AXL was measured by flow cytometry. AXL expression was measured by indirect immunofluorescence using 1H12-HAKB or B12 antibodies, followed by Alexa-488 anti-human secondary antibody (Life Technologies, Thermo Fisher Scientific). Cells were analyzed using an Accuri C6 Flow Cytometer (BD) equipped with a HyperCyt Autosampler (IntelliCyt), and data analyzed with FlowJo software (BD).

In vitro cytotoxicity and bystander assay

In vitro cytotoxicity was determined by incubation of cell lines with serial dilutions of ADCT-601, the nonbinding control ADC (B12-PL1601), or the free PBD dimer cytotoxin SG3199 for 5–8 days at 37°C in a 5% CO_2-gassed, humidified incubator. Cell viability was measured by CellTiterGlo luminescent cell viability assay (Promega), per manufacturer's instructions. Data were normalized to untreated control cells. The 50% inhibitory concentration (IC_{50}) values were determined using GraphPad (GraphPad Software) and mean and standard errors (SEs) of the means of three independent IC_{50} values were determined. For the bystander assay, AXL-positive SN12C cells and AXL-negative Karpas-299 cells were selected, as both are sensitive to the free PBD dimer cytotoxin SG3199, but only SN12C cells are killed by ADCT-601 with high sensitivity. Both cell lines were incubated with serial dilutions of ADCT-601 or B12-PL1601 for 5 days. Conditioned media were transferred from these initial cultures to fresh cultures of Karpas-299 cells, which were incubated for 5 days. Cell viability was measured in initial and secondary cultures by CellTiterGlo assay, as described above.

Internalization and colocalization studies

SN12C and MDA-MB-468 cells were incubated with either ADCT-601 or B12-PL1601 for 1 hour at 4°C, then incubated at 37°C where appropriate. Cells were fixed in 4% paraformaldehyde and permeabilized using 0.1% volume for volume (v/v) Tween-20 in PBS, washed with PBS, and centrifuged at 4,000 rpm (4°C). After removal of the supernatant, a rabbit mAb against lysosome-associated membrane protein 1 (LAMP-1;1:400; Cell Signaling Technology) was added and the cells were kept on ice for 1 hour before being washed. Secondary antibodies were added to detect ADCT-601 (Alexa Fluor 488 Goat

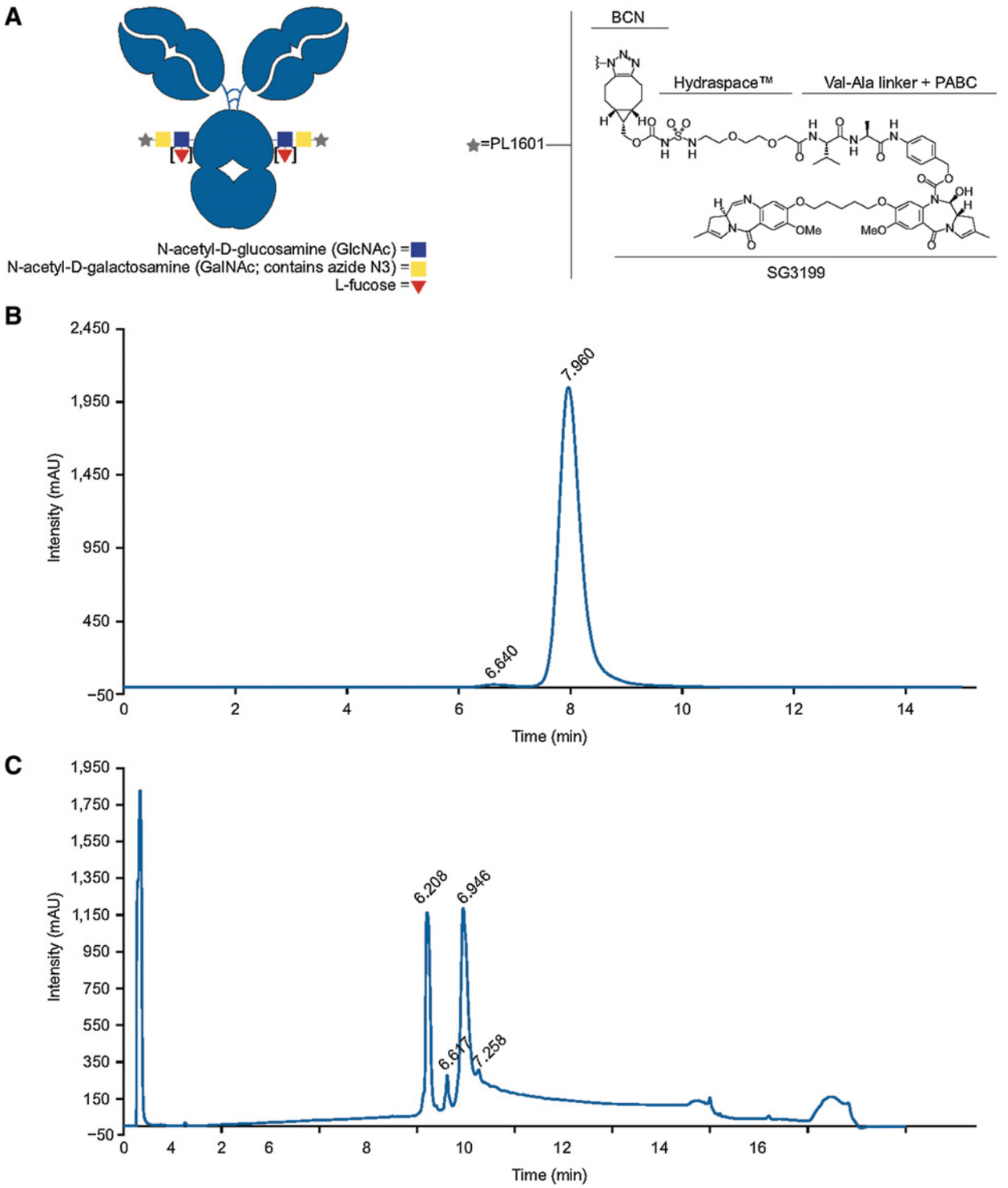

Figure 1.

Structure and characterization of ADCT-601. **A,** Structure of ADCT-601. **B,** ADCT-601 characterized by size exclusion chromatography. Results over the two injections were 1.2% high-molecular weight species/aggregates, 98.8% main product, and no detectable low-molecular weight species/others. **C,** Reduced reverse-phase liquid chromatography depicting reduced heavy and light chains of ADCT-601. BCN, bicyclo[6.1.0]non-4-yne; PABC, p-aminobenzyloxycarbonyl.

Anti-Human; 1:200; Thermo Fisher Scientific) and lysosomes (Alexa Fluor 568 Goat Anti-Rabbit; 1:200; Thermo Fisher Scientific), and the cells were incubated for 1 hour on ice. After a further wash, nuclei were counterstained with Hoechst 33342 (Thermo Fisher Scientific), cytospins of cell samples were prepared, and samples were visualized by immunofluorescence microscopy (Zeiss LSM 880).

In vitro DNA interstrand cross-linking determination

In vitro DNA ICLs were quantified using the single-cell gel electrophoresis (comet) assay, as described previously (33, 35). Briefly, SN12C or MDA-MB-468 cell lines were incubated with ADCT-601, B12-PL1601, or the free PBD dimer cytotoxin SG3199 for 2 hours at 37°C; then cells were washed, resuspended, and incubated at 37°C for 36 hours. ADCT-601, B12-PL1601 or SG3199 treated cells were irradiated (15 Gy) and kept on ice. Cells were stained with propidium iodide and visualized under epifluorescence microscope staining; the resulting image resembles a "comet" with a distinct head and tail. The Olive tail moment (OTM), defined as the product of tail length and fraction of total DNA in the tail, was evaluated by Komet 6 software (Andor Technology). Percentage reduction in OTM observed in cells treated with ADCT-601, B12-PL1601 or SG3199 was calculated and compared with untreated cells to indirectly quantify the level of cross-linked DNA.

Assessment of ADCT-601 efficacy in *in vivo* models

All animal studies were performed in facilities accredited by the Association for Assessment and Accreditation of Laboratory Animal Care, which assures compliance with accepted standards for the care and use of laboratory animals.

MDA-MB-231 and PAXF1657 xenografts were developed in female athymic nude mice by implanting 5×10^6 MDA-MB-231 cells and 3- to 4-mm edge length PAXF1657 fragments subcutaneously into their flanks, respectively. SN12C and Karpas-299 xenograft models were developed in female C.B-17 severe combined immunodeficient mice by implanting 5×10^6 SN12C cells and 1×10^7 Karpas-299 cells subcutaneous in their flanks, respectively. The ES0195 patient-derived xenograft (PDX) model [AXL $\log_2$(FPKM) 4.47; Crown Bioscience] was developed in female BALB/c nude mice by implanting 2- to 3-mm-diameter tumor fragments subcutaneously into their flanks. The NCI-H1299 xenograft model was developed in female athymic nude mice by implanting 1×10^7 cells subcutaneously into their flanks.

Mice were randomly allocated into groups of 7–10 animals (depending on experiment) to receive intravenous ADCT-601, an isotype-control ADC, vehicle, or AXL-107-MMAE when group mean tumor volumes reached a specified volume. After dosing on day 1, tumors were measured twice weekly using calipers; and each animal was euthanized when its tumor reached the specified endpoint volume or at study end, whichever came first. Data represent mean tumor volume ± SE. The time to end point (TTE) for analysis was calculated for each mouse using the following equation:

$$\text{TTE (days)} = (\log_{10}(\text{endpoint volume} - \text{intercept}^*)/\text{slope}^*)$$

In this equation, the asterisk (*) indicates the line obtained by linear regression of a log-transformed tumor growth dataset. The difference between the overall survival experiences (survival curves) of two groups based on their TTE values was assessed by log-rank test.

ADCT-601 in combination with olaparib

Combination of ADCT-601 and olaparib was tested in the ovarian cancer PDX CTG-0703. Olaparib was provided by Champions Oncology Inc.

CTG-0703–implanted athymic nude mice ($n = 8$/group), after reaching tumor volumes of 150–300 mm^3, were administered vehicle orally once a day ×28, olaparib 50 mg/kg orally once a day ×28, single-dose ADCT-601 0.15 mg/kg i.v., or the combination of single-dose ADCT-601 0.15 mg/kg i.v. + olaparib 50 mg/kg orally once a day ×28. Tumor volumes and body weights were measured twice weekly.

The coefficient of drug interaction (CDI) was assessed for sub-additive, additive, or supra-additive (synergism) properties on the last day when at least 50% of the animals remained on study, as described previously (36).

An animal was classified as a partial responder (PR) when tumor volume was ≤50% of its day 1 volume for three consecutive measurements during the course of the study, and ≥13.5 mm^3 for one or more of these three measurements. In a complete regression (CR) response, the tumor volume was <13.5 mm^3 for three consecutive measurements during the course of the study. An animal with a CR response at the termination of a study was additionally classified as a tumor-free survivor (TFS). Treatment tolerability was assessed by body weight measurements and by frequent observation for clinical signs of treatment-related side effects.

IHC of tumor xenografts

Human AXL expression in formalin-fixed paraffin-embedded (FFPE) tumor sections from PAXF1657 PDXs was detected using the BenchMark Ultra (Roche) staining system. Briefly, parental mouse monoclonal anti-human AXL antibody [ADC Therapeutics (UK) Limited] was applied for 30 minutes at 1:50 dilution following antigen retrieval of sections using CC1 solution (Ventana) for 60 minutes and a peroxidase (3%–4% v/v) blocking step. Detection of anti-AXL antibody was performed using the ultraView DAB detection kit (catalog no. 760-500; Roche).

Safety and tolerability

Safety and tolerability of ADCT-601 in non–tumor-bearing male Sprague-Dawley rats were determined following single-dose administration of ADCT-601 3 and 6 mg/kg. Necropsy was performed on day 21; and changes in body weight, hematologic, and histopathologic parameters were observed in different dose groups. The MTD was also determined.

Pharmacokinetic analysis in rats

Pharmacokinetic analysis of ADCT-601 was performed in non–tumor-bearing male Sprague-Dawley CD/IS rats. Serum samples were collected at predefined timepoints over a study period of 504 hours, after a single dose of 3 or 6 mg/kg. Quantitation of total (PBD-conjugated and -unconjugated) antibody, AXL antigen-binding antibody, and PBD-conjugated antibody was performed by electrochemiluminescence immunoassay analyzer using a biotinylated anti-human IgG-Fc antibody, an AXL antigen, and a biotinylated anti-PBD mouse antibody as a capture, respectively. For the total and AXL-binding antibody assays, anti-human IgG-Fc-sulfotag–conjugated antibody was used for detection, whereas for the PBD-conjugated antibody assay, an anti-idiotypic sulfotag-conjugated antibody was used. Streptavidin MSD plates were used for the biotinylated capture reagents and a standard plate for the AXL antigen capture reagent. A step-by-step approach was taken for all three assays with wash steps in between; the coating of capture reagent was followed by the addition of serum sample, with subsequent addition of detection reagent and then read buffer, after which the plate was read on an MSD QuickPlex Plate Reader (MSD). Toxicokinetic analysis by noncompartmental analysis was performed using Phoenix WinNonlin (Certara).

Results

Synthesis and characterization of ADCT-601

The humanized anti-human AXL antibody 1H12-HAKB was conjugated to PL1601 via GlycoConnect™ technology to produce ADCT-601. PL1601 consists of HydraSpace™, a polar sulfamide moiety, a protease cleavable Val-Ala linker and the PBD dimer cytotoxin SG3199 (**Fig. 1A**).

ADCT-601 was 98.8% monodisperse as determined by size exclusion chromatography (**Fig. 1B**). Drug-to-antibody ratio was 1.96, as determined by reverse-phase liquid chromatography (**Fig. 1C**).

Antibody binding

The 1H12-HAKB antibody demonstrated strong and specific binding to recombinant human AXL, while it did not bind to the other two TAM receptors, TYRO3 and MER (Supplementary Fig. S1).

1H12-HAKB and ADCT-601 bound to sAXL with similar affinities, indicating no binding affinity was lost by conjugating 1H12-HAKB to PL1601. K_D values of 1H12-HAKB and ADCT-601 for human sAXL were 0.211 and 0.311 nmol/L, respectively.

K_D measurements of 1H12-HAKB and ADCT-601 to the FcγRs and FcRn showed that conjugation of 1H12-HAKB to PL1601 completely abolished binding of ADCT-601 to huFcγRIIA and huFcγRIIB at the concentration tested, while it substantially decreased binding affinity to huFcγRI, huFcγRIIIA-158V, and huFcγRIIIA-158F. Binding to FcRn was comparable for 1H12-HAKB and ADCT-601 (Supplementary Table S2).

In vitro cytotoxicity

ADCT-601 selectively inhibited the growth of a panel of seven AXL-positive human cancer cell lines (Panc-1, A-172, SK-LU-1, MDA-MB-231, SK-OV-3, NCI-H1299, and SN12C), while no differential cytotoxicity with isotype-control ADC (B12-PL1601) was observed in two AXL-negative cell lines (MDA-MB-468 and Karpas299; **Table 1**). The PBD dimer cytotoxin SG3199 alone displayed potent cytotoxicity in all nine cancer cell lines, independent of AXL expression. No correlation was observed between AXL expression and either ADCT-601 or SG3199 cytotoxicity, with Pearson correlation coefficients of −0.55 ($P = 0.13$) and −0.0093 ($P = 0.98$), respectively. Notably, both ADCT-601 and SG3199 were active in the NSCLC-derived cell line NCI-H1299, which has been shown to be insensitive to an AXL-specific ADC conjugated to MMAE (i.e., AXL-107-MMAE ADC; ref. 25), likely due to reduced sensitivity to free MMAE and/or expression of multidrug resistance gene 1 (MDR1).

Internalization studies

AXL-positive SN12C cells incubated with ADCT-601 (1 hour at 4°C) showed strong cell surface binding ($T = 0$ hour; **Fig. 2A**). After a 1-hour incubation at 37°C, ADCT-601 internalization and colocalization with lysosomes was observed, as evidenced by costaining with the lysosomal marker LAMP-1. This colocalization was maintained at 2 hours and no evidence of residual ADC staining was observed at 24 hours, suggesting complete lysosomal degradation (**Fig. 2A**). In contrast, there was no evidence of membrane binding on treatment of SN12C cells with B12-PL1601, a nonbinding isotype-control ADC, and ADCT-601 did not bind or internalize in AXL-negative MDA-MB-468 cells (Supplementary Fig. S2).

Determination of *in vitro* DNA interstrand cross-linking

Following ADCT-601 binding to membranous AXL and its internalization and trafficking to lysosomes, the PL1601 linker-drug was cleaved, which released PBD dimer cytotoxin SG3199 inside the cells. After 2-hour incubation of SN12C cells with ADCT-601, a low level of DNA ICL (14.6%) was observed. DNA ICL levels increased over time, reaching a peak between 8 to 12 hours and persisted for up to 36 hours, indicating the induced DNA damage was neither detected nor repaired by DNA repair mechanisms during this period. Conversely, the DNA ICLs induced by free SG3199 reached a peak during the initial 2-hour incubation and DNA ICLs persisted for up to 36 hours. The isotype-control ADC, B12-PL1601, induced very low levels of DNA ICLs over the 36-hour time course (**Fig. 2B**).

In an AXL-negative cell line (MDA-MB-468), ADCT-601 and B12-PL1601 did not produce significant DNA ICLs over 36 hours. In contrast, the free SG3199 cytotoxin rapidly produced a high level of DNA ICLs, comparable with observations in the SN12C cell line (Supplementary Fig. S3).

ADCT-601 bystander effect

The ability of ADCT-601 to induce bystander killing of AXL-negative tumor cells was assessed via the conditioned medium transfer method. After AXL-positive SN12C cells and AXL-negative Karpas-299 cells were exposed to ADCT-601 and B12-PL1601, targeted AXL-specific cytotoxicity was observed in SN12C cells but not in Karpas-299 cells (ADCT-601 IC_{50} 0.042 nmol/L and 3.51 nmol/L in SN12C and Karpas-299 cells, respectively; isotype-control B12-PL1601 IC_{50} 1.62 nmol/L and 2.92 nmol/L in SN12C and Karpas-299 cells, respectively). When conditioned medium from SN12C or Karpas-299 cells treated with ADCT-601 was transferred to Karpas-299 cells, only the conditioned medium from ADCT-601–treated SN12C (IC_{50} 0.0159 nmol/L), but not Karpas-299 (IC_{50} 2.12 nmol/L), induced

Table 1. *In vitro* cytotoxicity and copy-number determination in a panel of cell lines.

	Panc-1	A-172	SK-LU-1	MDA-MB-231	SK-OV-3	NCI-H1299	SN12C	MDA-MB-468	Karpas-299
Copy number (±SE)	20,000 (± 8,340)	23,000 (± 3,910)	24,000 (± 3,996)	36,000 (± 6,257)	46,000 (± 8,488)	79,000 (± 9,276)	88,000 (± 6,882)	BLLQ	BLLQ
ADCT-601 IC_{50} nmol/L (±SE)	0.47 (± 0.05)	0.59 (± 0.08)	0.02 (± 0)	0.35 (± 0.06)	0.11 (± 0.02)	2.2 (± 0.05)	0.83 (± 0.12)	9.29 (± 0.12)	14.62 (± 0.22)
Isotype-control ADC IC_{50} nmol/L (±SE)	54.05 (± 6.23)	37.26 (± 3.13)	3.67 (± 0.19)	14.19 (± 0.56)	79.89 (± 1.82)	825 (± 427)	12.29 (± 0.47)	4.17 (± 0.04)	11.59 (± 0.27)
SG3199 IC_{50} pmol/L (±SE)	60.6 (± 3.83)	22.79 (± 1.61)	19.06 (± 1.37)	110.5 (± 10.24)	62.59 (± 6.36)	88.68 (± 7.58)	57.63 (± 5.27)	174.1 (± 29.09)	9.18 (± 0.45)

Note: Mean AXL molecules/cell in a panel of solid tumor cell lines and mean IC_{50} values of ADCT-601, isotype-control ADC, and PBD dimer cytotoxin SG3199. Data presented as mean ± SE, calculated from three independent experiments.

Abbreviations: ADC, antibody–drug conjugate; BLLQ, below lower limit of quantitation; IC_{50}, 50% inhibitory concentration; PBD, pyrrolobenzodiazepine; SE, standard error.

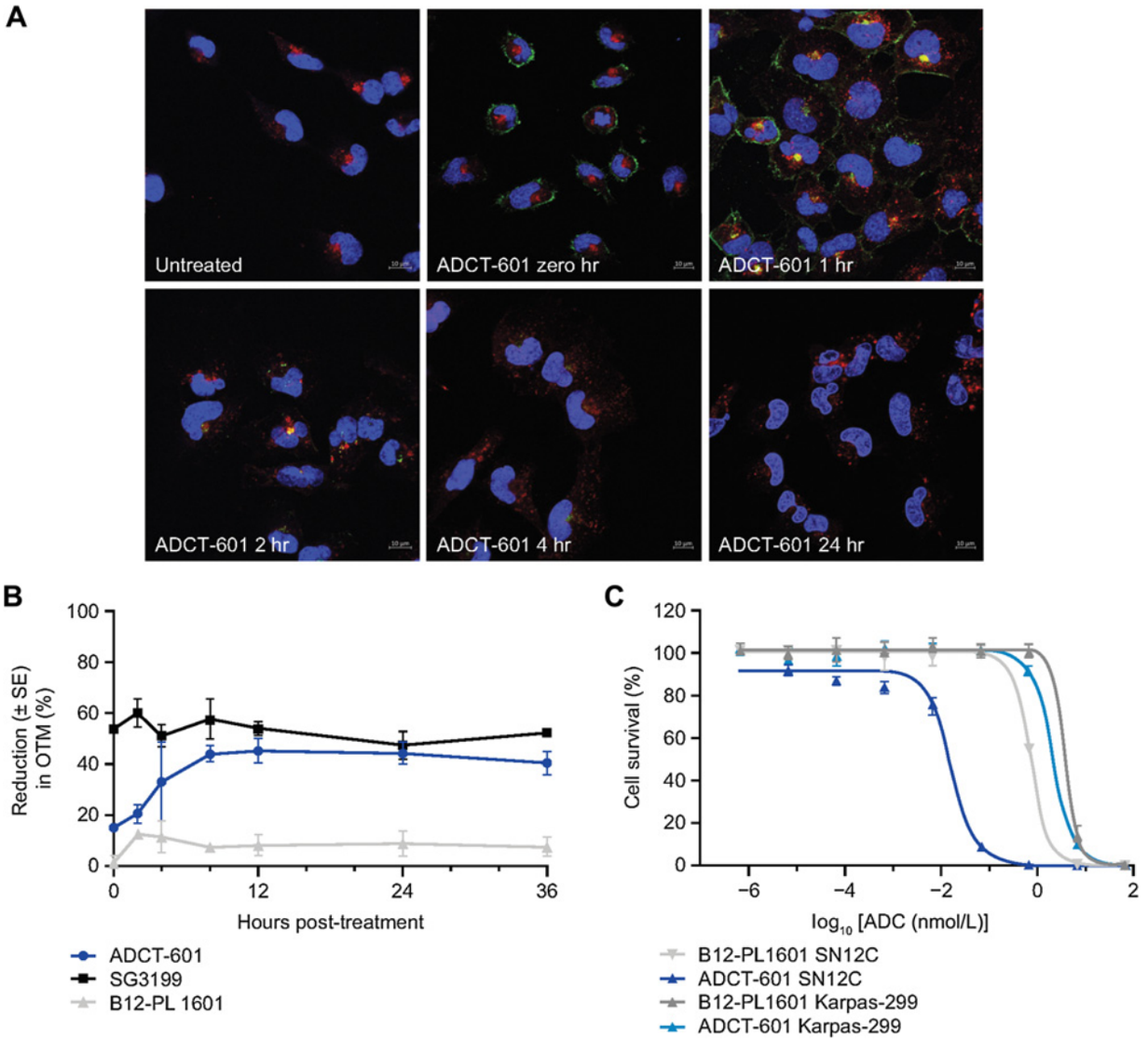

Figure 2.

Mechanism of action of ADCT-601. **A,** ADCT-601 internalization and lysosomal trafficking in SN12C cells, stained for nuclei (blue), LAMP-1 (red), and human IgG antibody (green). Costaining between LAMP-1 and IgG is observed as yellow. Scale bars, 10 μm. **B,** Time course of DNA ICL formation in SN12C cells by ADCT-601, B12-PL1601 or free PBD dimer cytotoxin SG3199. Results are presented as mean percentage decrease in OTM ± SE ($n = 3$). **C,** Bystander cytotoxicity of conditioned medium from SN12C and Karpas-299–treated cells transferred onto Karpas-299 cells. Data are presented as mean cytotoxicity IC_{50} values ± SE, calculated from three replica experiments. ADC, antibody–drug conjugate; IC_{50}, 50% inhibitory concentration; ICL, interstrand cross-links; IgG, immunoglobulin G; LAMP-1, lysosome-associated membrane protein 1; OTM, Olive tail moment; PBD, pyrrolobenzodiazepine; SE, standard error.

bystander killing of Karpas-299 cells. No bystander effect was observed when conditioned medium from B12-PL1601–treated SN12C cells or Karpas-299 cells was transferred onto untreated Karpas-299 cells (**Fig. 2C**).

Assessment of ADCT-601 efficacy in *in vivo* xenograft models

The antitumor activity of ADCT-601 was tested in a range of human solid tumor xenograft models covering multiple indications.

In the AXL-positive triple-negative breast cancer derived MDA-MB-231 xenograft model, a single dose of ADCT-601 at 1 mg/kg showed potent and sustained antitumor activity compared with vehicle and isotype-control ADC (**Fig. 3A**). ADCT-601 significantly increased survival versus isotype-control ADC (log-rank test, $P \leq 0.001$; Supplementary Fig. S4A), with 5/10 PR, 4/10 CR and 4/10 TFS in the ADCT-601–treated group, compared with no responses in the isotype-control ADC treated group on day 60 (Supplementary Table S3).

In the AXL-positive renal cancer derived SN12C xenograft model, a single dose of ADCT-601 (at 0.3, 0.6, and 1 mg/kg) had strong and dose-proportional antitumor activity (**Fig. 3B**). A significant increase in survival was observed in ADCT-601–treated mice compared with B12-PL1601–treated mice (log-rank test, ADCT-601 at each dose vs. B12-PL1601, $P \leq 0.001$; Supplementary Fig. S4B). At the highest dose tested (1 mg/kg ADCT-601), there

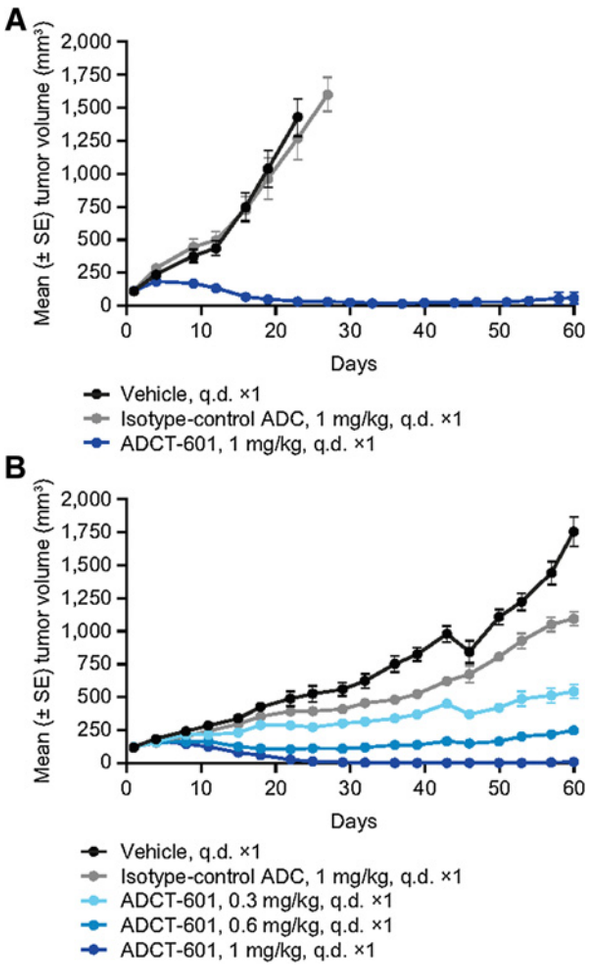

Figure 3.

In vivo antitumor activity of ADCT-601 in the MDA-MB-231 TNBC xenograft and in the SN12C renal cancer xenograft. **A,** *In vivo* antitumor activity of ADCT-601 in MDA-MB-231 TNBC xenograft model. Single-dose ADCT-601 and isotype-control ADC were administered intravenously (day 1) to treatment groups of 10 mice. A vehicle-treated group served as control. Data are shown as mean tumor volume ± SE. **B,** *In vivo* antitumor activity of ADCT-601 in SN12C renal cancer xenograft model. Single-dose ADCT-601 and isotype-control ADC (B12-PL1601) were administered intravenously (day 1) to treatment groups of 8 mice. A vehicle-treated group served as control. Data shown as mean tumor volume ± SE. ADC, antibody–drug conjugate; i.v., intravenously; q.d. ×1, once daily (dosing) for 1 day; SE, standard error; TNBC, triple-negative breast cancer.

were 1/8 PR, 7/8 CR, and 6/8 TFS at the end of the study (day 60), compared with no responses observed in vehicle-treated or B12-PL1601–treated mice (Supplementary Table S4).

ADCT-601 exhibited potent and dose-proportional antitumor activity when tested as a single low dose (at 0.075, 0.15, or 0.3 mg/kg) in a pancreatic cancer PDX model (PAXF1657) with heterogeneous AXL expression (**Fig. 4A**) and its activity was superior to AXL-107-MMAE, a MMAE-based AXL-specific ADC, when tested at the same dose of 0.3 mg/kg (**Fig. 4B**). AXL-107-MMAE tested at 4 mg/kg showed comparable antitumor activity, as previously reported in the same model (25). A significant increase in survival was observed with ADCT-601 versus AXL-107-MMAE (log-rank test, ADCT-601, 0.3 mg/kg vs. AXL-107-MMAE, 0.3 mg/kg, $P < 0.001$; **Fig. 4C**). There were 1/8 PR and 3/8 TFS in the ADCT-601 group versus no responses with a comparable dose of AXL-107-MMAE (Supplementary Table S5).

In the AXL-positive ES0195 esophageal cancer PDX model (37), ADCT-601 (1 mg/kg, single dose) showed strong and sustained antitumor activity compared with the control groups (vehicle and B12-PL1601; **Fig. 4D**), resulting in 5/8 PR, 2/8 CR, and 2/8 TFS at end of study (day 51), versus no responses observed in vehicle-treated or B12-PL1601–treated mice (Supplementary Table S6). A significant increase in survival was observed with ADCT-601 versus B12-PL1601 (log-rank test, ADCT-601 vs. B12-PL1601, $P \leq 0.0001$; Supplementary Fig. S4C). Notably, in the same model, the AXL-107-MMAE ADC was only able to induce temporary tumor regression when dosed twice at 4 mg/kg (37). Finally, in the AXL-negative Karpas-299 xenograft model, a single dose of ADCT-601 (1 mg/kg) had no significant antitumor activity compared with the vehicle group and did not result in increased survival (log-rank test, ADCT-601, 1 mg/kg vs. vehicle; $P =$ not significant; Supplementary Fig. S5; Supplementary Table S7). In all models, treatments were well tolerated, with minimal body weight loss (Supplementary Fig. S6) and no clinical observations reported.

In vivo activity of ADCT-601 in an MMAE-resistant xenograft model and in combination with olaparib in a BRCA1-mutated ovarian cancer PDX

To confirm the *in vitro* finding in the MMAE-resistant NCI-H1299 cell line (**Table 1**), single low doses of ADCT-601 were tested in mice implanted subcutaneously with NCI-H1299 cells. ADCT-601 showed antitumor activity at both doses tested (**Fig. 5A**) and both doses resulted in significantly increased survival compared with the isotype-control ADC, B12-PL1601 (log-rank test, $P < 0.05$; **Fig. 5B**). No dose–response relationship was observed for ADCT-601 in this model.

PBD-based ADCs have been shown to have enhanced efficacy when combined with olaparib, a PARP inhibitor, in BRCA-deficient tumors (38). To test whether the combination of ADCT-601 with olaparib increases antitumor activity, we assessed both agents in the AXL-expressing, BRCA1-mutated, CTG-0703 ovarian cancer PDX. Neither olaparib nor ADCT-601 exhibited significant antitumor activity compared with vehicle control when tested as single agents (**Fig. 5C**); however, their combination resulted in synergistic antitumor activity (CDI: 0.69; **Fig. 5C**) and significant antitumor activity compared with the vehicle control group (one-way ANOVA followed by Tukey multiple comparisons test, $P = 0.0099$). Importantly, the combination of ADCT-601 with olaparib was well tolerated with no body weight loss in any of the treated mice (**Fig. 5D**).

Assessment of ADCT-601 safety and tolerability in rats

ADCT-601 was well tolerated at doses of up to 6 mg/kg in rats, as assessed by clinical observation and standard toxicology criteria, including body weight, over 21 days. The off-target toxicity profile consisted of dose-dependent reductions in body weight (associated with reduced food consumption; Supplementary Fig. S7A) and reversible dose-dependent reductions in most blood cell populations (Supplementary Table S8A).

Pharmacokinetic analysis of ADCT-601 in rats

The pharmacokinetic profiles of total and PBD-conjugated antibody as well as AXL-binding antibody were determined in rats, a non–cross-reactive species to ADCT-601, following a single intravenous administration of ADCT-601 at 3 or 6 mg/kg

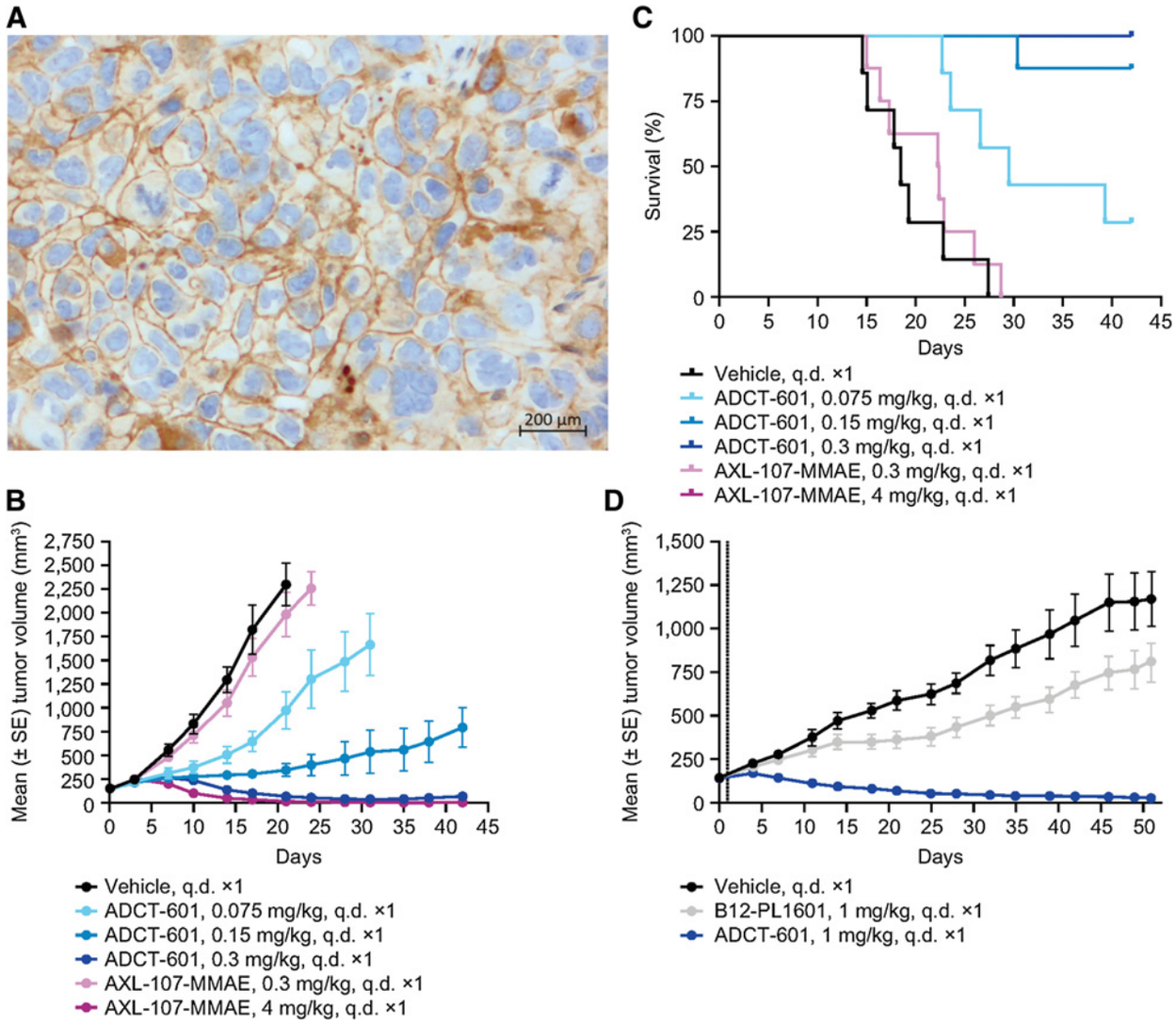

Figure 4.

In vivo antitumor activity of ADCT-601 in the PAXF1657 pancreatic cancer PDX and ES0195 esophageal cancer PDX. **A,** Representative scan of FFPE PAXF1657 tumor section stained for AXL by IHC. Scale bar, 200 µm. **B,** *In vivo* antitumor activity of ADCT-601 in PAXF1657 pancreatic cancer PDX model in comparison with AXL-107-MMAE ADC. Single-dose ADCT-601, AXL-107-MMAE ADC and isotype-control ADC (B12-PL1601) were administered intravenously (day 1) to treatment groups of 8 mice. A vehicle-treated group served as control. Data shown as mean tumor volume ± SE. **C,** Kaplan–Meier survival plots show percentage animal survival over 45 days after administration of a single dose of ADCT-601, AXL-107-MMAE ADC, or isotype-control ADC (B12-PL1601); ADCT-601, 0.3 mg/kg versus AXL-107-MMAE, 0.3 mg/kg, log-rank test, $P < 0.001$. The curve for AXL-107 MMAE 4 mg/kg is not visible owing to overlap with the curve for ADCT-601, 0.3 mg/kg. **D,** *In vivo* antitumor activity of ADCT-601 in ES0195 esophageal cancer PDX model. Single-dose ADCT-601 and isotype-control ADC (B12-PL1601) were administered intravenously (day 1) to treatment groups of 8 mice. A vehicle-treated group served as control. Data shown as mean tumor volume ± SE. ADC, antibody–drug conjugate; FFPE, formalin-fixed paraffin-embedded; IHC, immunohistochemistry; i.v., intravenous; MMAE, monomethyl auristatin E; PDX, patient-derived xenograft; q.d. ×1, once daily (dosing) for 1 day; SE, standard error.

(Supplementary Fig. S7B). ADCT-601 showed excellent stability *in vivo* with a half-life of 8.8, 9.2, and 9.5 days for total, AXL-binding, and PBD-conjugated antibody, respectively, at the 3 mg/kg dose, and 5.7, 5.8, and 5.7 days, respectively, at the 6 mg/kg dose (Supplementary Table S8B).

Discussion

AXL-targeted therapies may offer a novel therapeutic avenue for the treatment of cancer (2, 11), with antitumor efficacy mediated by prevention of AXL-mediated cancer development, progression, and resistance to therapy (22, 39, 40).

ADCT-601 (mipasetamab uzoptirine) is the first AXL-targeted ADC conjugated to a PBD dimer cytotoxin, thus combining the advantages of AXL-directed therapies with PBD-based technology. Recently, the first PBD dimer-based ADC, loncastuximab tesirine targeting CD19, was approved for relapsed/refractory DLBCL, showing the promise of highly potent PBD dimer-based ADCs for the treatment of advanced tumors as other CD19-targeted ADCs employing other toxins (such as auristatins and maytansins) have failed in this

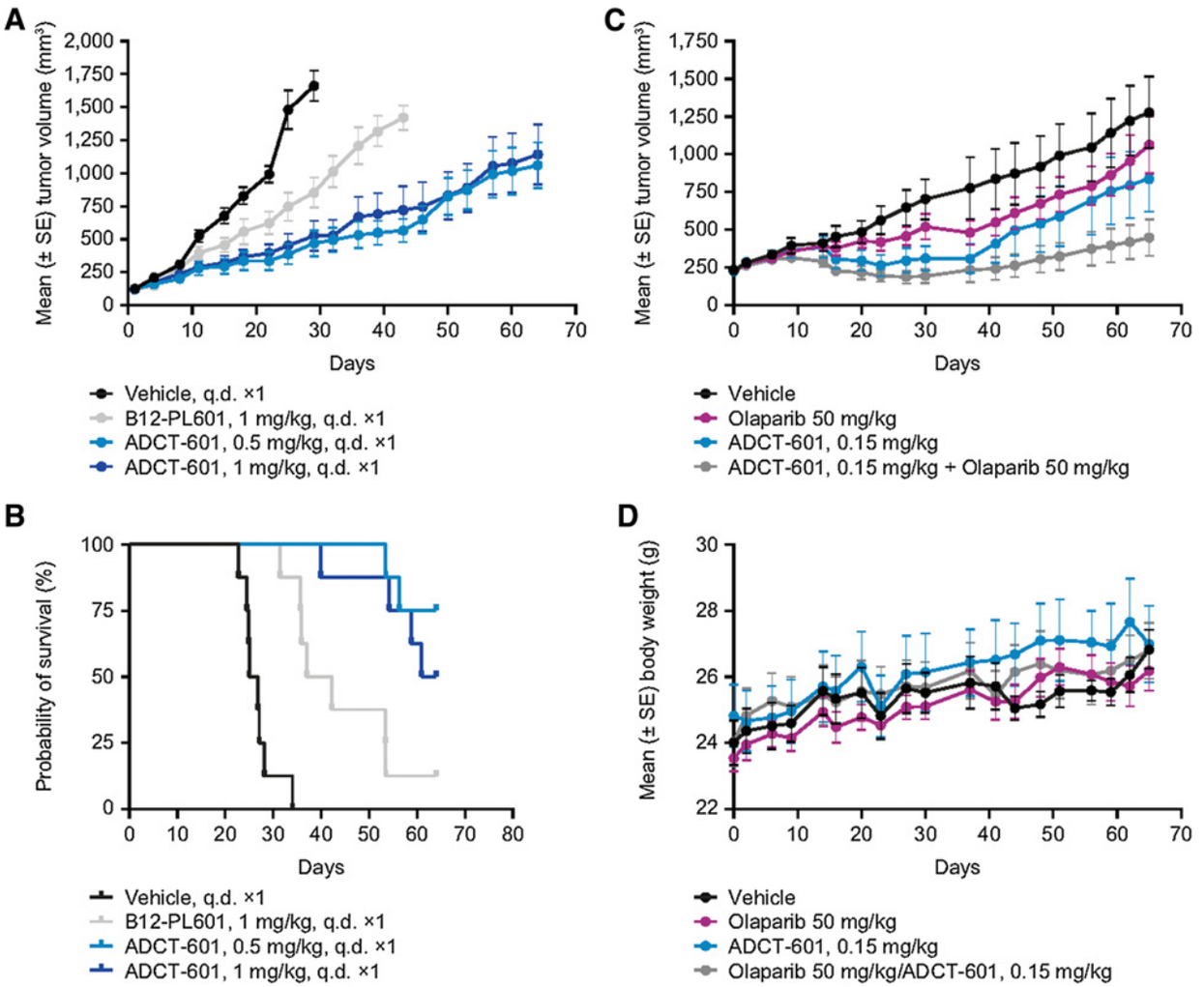

Figure 5.

In vivo antitumor activity of ADCT-601 in the MMAE-resistant NCI-H1299 NSCLC model, and in combination with olaparib in BRCA1-mutated ovarian cancer PDX. **A,** *In vivo* antitumor activity of ADCT-601 in a MMAE-resistant NCI-H1299 NSCLC model. Single-dose ADCT-601 and isotype-control ADC (B12-PL1601) were administered intravenously (day 1) to treatment groups of 8 mice. A vehicle-treated group served as control. Data are shown as mean tumor volume ± SE. **B,** Kaplan–Meier survival plot shows percentage animal survival over 60 days after administration of single-dose ADCT-601 or isotype-control ADC (B12-PL1601). ADCT-601 (both doses) versus B12-PL1601, log-rank test, $P < 0.05$. **C,** *In vivo* antitumor activity of ADCT-601 in combination with olaparib in the BRCA1-mutated ovarian cancer PDX model CTG-0703. Data shown as mean tumor volume ± SE. ADCT-601 + olaparib versus vehicle, one-way ANOVA followed by Tukey multiple comparisons test, $P = 0.0099$. **D,** Body weight in mice with BRCA1-mutated CTG-0703 ovarian cancer. Data shown as mean body weight (g) ± SE. ADC, antibody–drug conjugate; i.v., intravenous; MMAE, monomethyl auristatin E; NSCLC, non–small cell lung cancer; PDX, patient-derived xenograft; q.d. ×1, once daily (dosing) for 1 day; SE, standard error.

setting. ADCT-601 acts by binding to human AXL and releasing the PBD dimer cytotoxin SG3199 at the target site inside the cell, which causes tumor cell death as a result of cytotoxic DNA ICLs (33, 34). The data presented herein show that ADCT-601 is a highly potent AXL-targeted ADC active against a range of solid tumor cell lines expressing different levels of AXL. ADCT-601 cytotoxicity required AXL expression on the surface of the tumor cells, although, in the cell line panel analyzed, no correlation was noted between AXL copy number and ADCT-601 IC_{50}, potentially due to the cell lines different sensitivity to SG3199. ADCT-601 bound to sAXL, which is reported to be elevated in serum of patients with cancer (8, 41), therefore measurement of sAXL may represent an important biomarker for the pharmacokinetics and pharmacodynamics of ADCT-601 in patients with cancer.

ADCT-601 was rapidly internalized by AXL-expressing cells and colocalization images suggest that processing of ADCT-601 is lysosomal in nature. Following incubation with ADCT-601, DNA ICLs formation peaked between 8 to 12 hours and persisted for up to 36 hours, suggesting that the DNA damage induced by ADCT-601 is neither detected nor repaired by DNA repair mechanisms during this period, which could contribute to its sustained antitumor activity.

For ADCT-601 to be effective in cancer with heterogenous AXL expression, bystander activity on target-negative cancer cells is required for tumor eradication. To enable this, the PBD cytotoxin released from the target-positive cells must be diffusible and exert cytotoxicity in the target-negative cells (33, 34). Conditioned medium

transfer experiments confirmed bystander killing of AXL-negative Karpas-299 cells by a soluble factor released from AXL-positive, ADCT-601–treated SN12C cells into the medium; this soluble factor is assumed to be the PBD dimer cytotoxin SG3199, released by cleavage of ADCT-601.

In vivo, single low doses of ADCT-601 resulted in remarkable, sustained antitumor activity and significantly improved survival across a panel of tumor models spanning triple-negative breast, renal, pancreatic, and esophageal cancer–derived xenografts expressing different levels of AXL. Interestingly, in the PAXF1657 model, a pancreatic cancer PDX with heterogeneous AXL expression, a single low dose of ADCT-601 resulted in complete tumor eradication, indicating potent and durable anticancer activity of ADCT-601, possibly mediated by *in vivo* bystander killing. Furthermore, comparison with the auristatin-based AXL-specific ADC AXL-107-MMAE suggested superiority of ADCT-601 in this model.

Upregulation of the drug transporter P-glycoprotein (ABCB1, MDR1) is one of the most commonly upregulated efflux pumps associated with small-molecule drug resistance and MDR1 has been implicated in acquired resistance to ADCs such as trastuzumab emtansine, gemtuzumab ozogamicin, and inotuzumab ozogamicin (42–45). Interestingly, MDR1 was not found to be significantly upregulated in two cancer cell lines with acquired resistance to either PBD-containing ADCs or SG3199 (46), the PBD cytotoxin component of ADCT-601, although SG3199 was previously found to be moderately susceptible to multidrug resistance mechanisms in human tumor cell lines expressing MDR1 (47). In this study, ADCT-601 was active both *in vitro* and *in vivo* in the NCI-H1299 model, a NSCLC-derived cell line expressing MDR1 in which AXL-107-MMAE is inactive (25).

The combination of a PBD-based ADC with the PARP inhibitor olaparib has been shown to significantly enhance the antitumor effect compared with monotherapy in mice bearing BRCA2-deleted tumors (38). Here we show the potent preclinical antitumor activity of ADCT-601 in combination with olaparib: the combination of a suboptimal dose of ADCT-601 with olaparib resulted in synergistic antitumor activity in a BRCA1-mutated ovarian cancer PDX and was well tolerated in mice. The synergistic antitumor activity of ADCT-601 with olaparib bodes well for the translation of these findings in treating patients with BRCA-deficient cancers expressing AXL.

AXL upregulation has been reported in multiple tumor types after they have become resistant to conventional and targeted therapies such as erlotinib, sunitinib, lapatinib, and imatinib (15–19). Hence, ADCT-601 could be used to treat patients who have become resistant to targeted therapies and have consequently increased AXL expression. AXL is also expressed on multiple immune cell types in the tumor immune microenvironment where it promotes a suppressive myeloid microenvironment. Therefore, ADCT-601–mediated depletion of AXL-expressing, immunosuppressive immune cells could combine well with checkpoint inhibitors and could result in synergistic antitumor efficacy, improving tumor eradication, as previously shown with a PBD-based ADC targeting CD25 (48). Moreover, given the known ability of PBD-based ADCs to induce immunogenic cell death and synergize *in vivo* with immuno-oncology therapies (49), it is possible that ADCT-601 will trigger immunogenic cell death in AXL-expressing tumors or immune bystander cells, attracting immune cells to the tumor site and ultimately synergizing with immuno-oncology drugs. Studies investigating ADCT-601's ability to target AXL-positive immune cells are currently ongoing.

ADCT-601 utilizes both the GlycoConnect™ and HydraSpace technologies. GlycoConnect™ is based on a chemoenzymatic strategy that allows specific attachment of the cytotoxin to remodeled N-linked glycans located in the Fc pocket of the immunoglobulins. On the basis of preclinical data, GlycoConnect™ combined with the polar spacer HydraSpace™ provides ADCs with an enhanced therapeutic index compared with ADCs manufactured by random conjugation processes (27, 28, 50). In our study, ADCT-601 had a favorable off-target safety profile in rats, with a MTD of 6 mg/kg, exceeding the rat MTD for other SG3199-based ADCs by approximately 4-fold (34) and for 1H12-HAKB stochastically conjugated to SG3249 (data on file).

Moreover, GlycoConnect™ conjugation technology resulted in a stable ADC, as shown by the pharmacokinetic profile of ADCT-601 in rats, indicating excellent stability and a half-life consistent with the expected profile for an IgG1 antibody/ADC in a nonbinding species.

In conclusion, ADCT-601 efficiently and specifically inhibits *in vitro* and *in vivo* cell growth of AXL-positive human cancer cell lines and tumor xenograft models, both as monotherapy or in combination with olaparib, providing a strong rationale for its use in the treatment of AXL-expressing tumors and demonstrating that the preclinical data reported here warrant further evaluation of ADCT-601 in the clinical setting.

Authors' Disclosures

F. Zammarchi was employed by ADC Therapeutics at the time the work was conducted, and holds shares/stocks in ADC Therapeutics. K.E. Havenith reports personal fees from ADC Therapeutics during the conduct of the study; other support from ADC Therapeutics outside the submitted work. P. Hogg was employed by ADC Therapeutics at the time the work was conducted and holds shares/stocks in ADC Therapeutics. P. Tyrer was an employee of Spirogen/AstraZeneca when the work was performed. J.A. Hartley reports grants and personal fees from ADC Therapeutics during the conduct of the study; personal fees from AstraZeneca outside the submitted work. P.H. van Berkel reports a patent for ADCT-601 pending. S. Chivers, P. van Berkel and K. Havenith were employed by ADCT during the conduct of the study and F. Bertelli was employed by AstraZeneca. No disclosures were reported by the other authors.

Authors' Contributions

F. Zammarchi: Conceptualization, formal analysis, supervision, writing–original draft, writing–review and editing. **K.E. Havenith:** Data curation, methodology. **S. Chivers:** Supervision. **P. Hogg:** Methodology. **F. Bertelli:** Resources, data curation, investigation, methodology, writing–review and editing. **P. Tyrer:** Resources, data curation, investigation, methodology, writing–original draft. **N. Janghra:** Investigation, visualization, methodology. **H.W. Reinert:** Visualization, methodology. **J.A. Hartley:** Conceptualization, supervision, methodology, writing–review and editing. **P.H. van Berkel:** Conceptualization, supervision, writing–original draft.

Acknowledgments

These preclinical studies were funded by ADC Therapeutics (UK) Limited.

The authors thank Charles River Discovery Research Services (USA and Germany GmbH), Crown Bioscience Inc. (USA) and Champions Oncology (USA) for conducting the *in vivo* studies, Synaffix BV (The Netherlands), Sterling Pharma Solutions (Wales, United Kingdom) for support with the conjugation, and ADC Therapeutics pharmacokinetic team (London, United Kingdom) for conducting the pharmacokinetic assay. Medical writing support was provided by Heather St Michael and Emiliana Jelezarova at Fishawack Communications Ltd, part of Fishawack Health, funded by ADC Therapeutics (United Kingdom) Limited.

The costs of publication of this article were defrayed in part by the payment of page charges. This article must therefore be hereby marked *advertisement* in accordance with 18 U.S.C. Section 1734 solely to indicate this fact.

Received August 24, 2021; revised November 13, 2021; accepted January 18, 2022; published first January 27, 2022.

References

1. Paccez JD, Vogelsang M, Parker MI, Zerbini LF. The receptor tyrosine kinase Axl in cancer: biological functions and therapeutic implications. Int J Cancer 2014; 134:1024–33.
2. Gay CM, Balaji K, Byers LA., Giving AXL the axe: targeting AXL in human malignancy. Br J Cancer 2017;116:415–23.
3. Li Y, Ye X, Tan C, Hongo J-A, Zha J, Liu J, et al. Axl as a potential therapeutic target in cancer: role of Axl in tumor growth, metastasis and angiogenesis. Oncogene 2009;28:3442–55.
4. May CD, Garnett J, Ma X, Landers SM, Ingram DR, Demicco EG, et al. AXL is a potential therapeutic target in dedifferentiated and pleomorphic liposarcomas. BMC Cancer 2015;15:901.
5. Shieh YS, Lai C-Y, Kao Y-R, Shiah S-G, Chu Y-W, Lee H-S, et al. Expression of axl in lung adenocarcinoma and correlation with tumor progression. Neoplasia 2005;7:1058–64.
6. Ben-Batalla I, Schultze A, Wroblewski M, Erdmann R, Heuser M, Waizenegger JS, et al. Axl, a prognostic and therapeutic target in acute myeloid leukemia mediates paracrine crosstalk of leukemia cells with bone marrow stroma. Blood 2013;122:2443–52.
7. Hutterer M, Knyazev P, Abate A, Reschke M, Maier H, Stefanova N, et al. Axl and growth arrest–specific gene 6 are frequently overexpressed in human gliomas and predict poor prognosis in patients with glioblastoma multiforme. Clin Cancer Res 2008;14:130–8.
8. Rankin EB, Giaccia AJ., The receptor tyrosine kinase AXL in cancer progression. Cancers 2016;8:103.
9. Byers LA, Diao L, Wang J, Saintigny P, Girard L, Peyton M, et al. An epithelial-mesenchymal transition gene signature predicts resistance to EGFR and PI3K inhibitors and identifies Axl as a therapeutic target for overcoming EGFR inhibitor resistance. Clin Cancer Res 2013;19:279–90.
10. Gjerdrum C, Tiron C, Hoiby T, Stefansson I, Haugen H, Sandal T, et al. Axl is an essential epithelial-to-mesenchymal transition-induced regulator of breast cancer metastasis and patient survival. Proc Natl Acad Sci U S A 2010;107: 1124–9.
11. Wu X, Liu X, Koul S, Lee CY, Zhang Z, Halmos B. AXL kinase as a novel target for cancer therapy. Oncotarget 2014;5:9546–63.
12. Aguilera TA, Rafat M, Castellini L, Shehade H, Kariolis MS, Hui AB-Y, et al. Reprogramming the immunological microenvironment through radiation and targeting Axl. Nat Commun 2016;7:13898.
13. Yule M, Davidsen K, Bloe M, Hodneland L, Engelsen A, Lie M, et al. Combination of bemcentinib (BGB324)–a first-in-class selective, oral AXL inhibitor–with pembrolizumab in patients with triple negative breast cancer and adenocarcinoma of the lung. J Clin Oncol 36: 15s, 2018 (suppl; abstr TPS43).
14. Schoumacher M, Burbridge M., Key roles of AXL and MER receptor tyrosine kinases in resistance to multiple anticancer therapies. Curr Oncol Rep 2017; 19:19.
15. Morgillo F, Della Corte CM, Fasano M, Ciardiello F. Mechanisms of resistance to EGFR-targeted drugs: lung cancer. ESMO Open 2016;1:e000060.
16. Zhang Z, Lee JC, Lin L, Olivas V, Au V, LaFramboise T, et al. Activation of the AXL kinase causes resistance to EGFR-targeted therapy in lung cancer. Nat Genet 2012;44:852–60.
17. Zhou L, Liu X-D, Sun M, Zhang X, German P, Bai S, et al. Targeting MET and AXL overcomes resistance to sunitinib therapy in renal cell carcinoma. Oncogene 2016;35:2687–97.
18. Dufies M, Jacquel A, Belhacene N, Robert G, Cluzeau T, Luciano F, et al. Mechanisms of AXL overexpression and function in Imatinib-resistant chronic myeloid leukemia cells. Oncotarget 2011;2:874–85.
19. Liu L, Greger J, Shi H, Liu Y, Greshock J, Annan R, et al. Novel mechanism of lapatinib resistance in HER2-positive breast tumor cells: activation of AXL. Cancer Res 2009;69:6871–8.
20. Macleod K, Mullen P, Sewell J, Rabiasz G, Lawrie S, Miller E, et al. Altered ErbB receptor signaling and gene expression in cisplatin-resistant ovarian cancer. Cancer Res 2005;65:6789–800.
21. Wu G, Ma Z, Cheng Y, Hu W, Deng C, Jiang S, et al. Targeting Gas6/TAM in cancer cells and tumor microenvironment. Mol Cancer 2018;17:20.
22. Holland SJ, Pan A, Franci C, Hu Y, Chang B, Li W, et al. R428, a selective small molecule inhibitor of Axl kinase, blocks tumor spread and prolongs survival in models of metastatic breast cancer. Cancer Res 2010;70:1544–54.
23. Aehnlich P, Powell RM, Peeters MJW, Rahbech A, thor Straten P. TAM receptor inhibition-implications for cancer and the immune system. Cancers 2021;13: 1195.
24. Khongorzul P, Ling CJ, Khan FU, Ihsan AU, Zhang J. Antibody-drug conjugates: a comprehensive review. Mol Cancer Res 2020;18:3–19.
25. Boshuizen J, Koopman LA, Krijgsman O, Shahrabi A, van den Heuvel EG, Ligtenberg MA, et al. Cooperative targeting of melanoma heterogeneity with an AXL antibody-drug conjugate and BRAF/MEK inhibitors. Nat Med 2018;24: 203–12.
26. Sharp LL, Chang C, Frey G, Wang J, Liu H, Xing C, et al. Anti-tumor efficacy of BA3011, a novel conditionally active biologic (CAB) anti-AXL-ADC [abstract]. In: Proceedings of the American Association for Cancer Research Annual Meeting 2018; 2018 Apr 14–18; Chicago, IL. Philadelphia (PA): AACR; Cancer Res 2018;78(13 Suppl):Abstract nr 827. https://cancerres.aacrjournals.org/content/78/13_supplement/2792a.abstract.
27. Verkade J, Wijdeven M, Janssen B. A polar sulfamide spacer significantly enhances the manufacturability, stability, and therapeutic index of antibody–drug conjugates. Antibodies 2018;7:12.
28. van Geel R, Wijdeven MA, Heesbeen R, Verkade JMM, Wasiel AA, van Berkel SS, et al. Chemoenzymatic conjugation of toxic payloads to the globally conserved N-Glycan of native mabs provides homogeneous and highly efficacious antibody-drug conjugates. Bioconjug Chem 2015;26:2233–42.
29. Zammarchi F, et al. Preclinical activity of ADCT-601, a novel pyrrolobenzodiazepine (PBD) dimer-based antibody-drug conjugate (ADC) targeting AXL-expressing tumors. Abstract 2792A, AACR Annual Meeting, April 14–18, 2018, Chicago, IL. https://cancerres.aacrjournals.org/content/78/13_supplement/2792a.abstract.
30. Hartley JA., Antibody-drug conjugates (ADCs) delivering pyrrolobenzodiazepine (PBD) dimers for cancer therapy. Expert Opin Biol Ther 2021;21:931–43.
31. Ahmed L, Kiprijanov SM, Nalwoga H, Wnuk-Lipinska K, Haugen H, Lorens JB, et al. Novel anti-human Axl monoclonal antibodies for improved patient biomarker studies. Diagnostic Pathol 2016;2:104.
32. Tiberghien AC, Levy J-N, Masterson LA, Patel NV, Adams LR, Corbett S, et al. Design and synthesis of tesirine, a clinical antibody-drug conjugate pyrrolobenzodiazepine dimer payload. ACS Med Chem Lett 2016;7:983–7.
33. Flynn MJ, Zammarchi F, Tyrer PC, Akarca AU, Janghra N, Britten CE, et al. ADCT-301, a pyrrolobenzodiazepine (PBD) dimer-containing antibody-drug conjugate (ADC) targeting CD25-expressing hematological malignancies. Mol Cancer Ther 2016;15:2709–21.
34. Zammarchi F, Corbett S, Adams L, Tyrer PC, Kiakos K, Janghra N, et al. ADCT-402, a PBD dimer-containing antibody drug conjugate targeting CD19-expressing malignancies. Blood 2018;131:1094–105.
35. Spanswick VJ, Hartley JM, Hartley JA., Measurement of DNA interstrand crosslinking in individual cells using the single cell gel electrophoresis (Comet) assay. Methods Mol Biol 2010;613:267–82.
36. Wu J, Tracey L, Davidoff AM., Assessing interactions for fixed-dose drug combinations in tumor xenograft studies. J Biopharm Stat 2012;22:535–43.
37. Antibodies binding AXL (WO2016005593). GENMAB A/S [DK/DK]; Bredgade 34 E 1260 Copenhagen K, DK; PCT/EP2015/065900 (2016).
38. Zhong H, Chen C, Tammali R, Breen S, Zhang J, Fazenbaker C, et al. Improved therapeutic window in BRCA-mutant tumors with antibody-linked pyrrolobenzodiazepine dimers with and without PARP Inhibition. Mol Cancer Ther 2019;18:89–99.
39. Balaji K, Vijayaraghavan S, Diao L, Tong P, Fan Y, Carey JPW, et al. AXL inhibition suppresses the DNA damage response and sensitizes cells to PARP inhibition in multiple cancers. Mol Cancer Res 2017;15:45–58.
40. Elkabets M, Pazarentzos E, Juric D, Sheng Q, Pelossof RA, Brook S, et al. AXL mediates resistance to PI3Kalpha inhibition by activating the EGFR/PKC/mTOR axis in head and neck and esophageal squamous cell carcinomas. Cancer Cell 2015;27:533–46.
41. Dengler M, Staufer K, Huber H, Stauber R, Bantel H, Weiss KH, et al. Soluble Axl is an accurate biomarker of cirrhosis and hepatocellular carcinoma development: results from a large scale multicenter analysis. Oncotarget 2017;8:46234–48.
42. Chen R, Hou J, Newman E, Kim Y, Donohue C, Liu X, et al. CD30 down-regulation, MMAE resistance, and MDR1 upregulation are all associated with resistance to brentuximab vedotin. Mol Cancer Ther 2015;14:1376–84.
43. Loganzo F, Tan X, Sung M, Jin G, Myers JS, Melamud E, et al. Tumor cells chronically treated with a trastuzumab-maytansinoid antibody-drug conjugate develop varied resistance mechanisms but respond to alternate treatments. Mol Cancer Ther 2015;14:952–63.
44. Sung M, Tan X, Lu B, Golas J, Hosselet C, Wang F, et al. Caveolae-mediated endocytosis as a novel mechanism of resistance to trastuzumab emtansine (T-DM1). Mol Cancer Ther 2018;17:243–53.

45. Walter RB, Gooley TA, van der Velden VHJ, Loken MR, van Dongen JJM, Flowers DA, et al. CD33 expression and P-glycoprotein-mediated drug efflux inversely correlate and predict clinical outcome in patients with acute myeloid leukemia treated with gemtuzumab ozogamicin monotherapy. Blood 2007;109: 4168–70.
46. Corbett S, Huang S, Zammarchi F, Howard PW, van Berkel PH, Hartley JA. The role of specific ATP-binding cassette transporters in the acquired resistance to pyrrolobenzodiazepine dimer-containing antibody-drug conjugates. Mol Cancer Ther 2020;19:1856–65.
47. Hartley JA, Flynn MJ, Bingham JP, Corbett S, Reinert H, Tiberghien A, et al. Pre-clinical pharmacology and mechanism of action of SG3199, the pyrrolobenzodiazepine (PBD) dimer warhead component of antibody-drug conjugate (ADC) payload tesirine. Sci Rep 2018;8: 10479.
48. Zammarchi F, Havenith K, Bertelli F, Vijayakrishnan B, Chivers S, van Berkel PH. CD25-targeted antibody-drug conjugate depletes regulatory T cells and eliminates established syngeneic tumors via antitumor immunity. J Immunother Cancer 2020;8:e000860.
49. Rios-Doria J, Harper J, Rothstein R, Wetzel L, Chesebrough J, Marrero A, et al. Antibody-drug conjugates bearing pyrrolobenzodiazepine or tubulysin payloads are immunomodulatory and synergize with multiple immunotherapies. Cancer Res 2017;77:2686–98.
50. van Delft F, Janssen B, van Geel R, Wijdeven M, Verkade J, van Berkel S, et al. Decomposition of parameters contributing to the improved therapeutic index of ADCs obtained by GlycoConnect™ and HydraSpace™ technologies [abstract]. In: Proceedings of the American Association for Cancer Research Annual Meeting 2018; 2018 Apr 14–18; Chicago, IL. Philadelphia (PA): AACR; Cancer Res 2018;78(13 Suppl):Abstract nr 3815.